



Experiments on the Resonance of Long-Period Waves Near Islands

Author(s): D. R. Caldwell and S. A. Eide

Source: *Proceedings of the Royal Society of London. Series A, Mathematical and Physical Sciences*, Vol. 348, No. 1654, (Mar. 9, 1976), pp. 359-378

Published by: The Royal Society

Stable URL: <http://www.jstor.org/stable/79128>

Accessed: 04/08/2008 12:45

Your use of the JSTOR archive indicates your acceptance of JSTOR's Terms and Conditions of Use, available at <http://www.jstor.org/page/info/about/policies/terms.jsp>. JSTOR's Terms and Conditions of Use provides, in part, that unless you have obtained prior permission, you may not download an entire issue of a journal or multiple copies of articles, and you may use content in the JSTOR archive only for your personal, non-commercial use.

Please contact the publisher regarding any further use of this work. Publisher contact information may be obtained at <http://www.jstor.org/action/showPublisher?publisherCode=rsl>.

Each copy of any part of a JSTOR transmission must contain the same copyright notice that appears on the screen or printed page of such transmission.

JSTOR is a not-for-profit organization founded in 1995 to build trusted digital archives for scholarship. We work with the scholarly community to preserve their work and the materials they rely upon, and to build a common research platform that promotes the discovery and use of these resources. For more information about JSTOR, please contact support@jstor.org.

Experiments on the resonance of long-period waves near islands

BY D. R. CALDWELL AND S. A. EIDE

*School of Oceanography, Oregon State University,
Corvallis, Oregon 97331, U.S.A.*

(Communicated by M.S. Longuet-Higgins, F.R.S.)

[Plates 3–9]

Rotating model studies of the resonant trapping of wave energy at periods longer than the inertial demonstrate this phenomenon for Kelvin- and shelf-type waves. Previous predictions for the resonant frequencies for the Kelvin-type waves are quantitatively confirmed. For the shelf-type waves systematic discrepancies are found between the experiments and the theoretical predictions. The effects of amplitude and horizontal scale on these waves are discussed, but no explanation for the discrepancies is found.

1. INTRODUCTION

Longuet-Higgins (1971) suggests that some of the peaks in the cospectrum of sea level at Honolulu and Mokuoloe computed by Miyata & Groves (1968) may represent long-period waves trapped by the bathymetry near Oahu, although the peaks at 0.35 and 0.25 c/d may be observations of normal modes of the Pacific Ocean basin. The analysis by Miyata & Groves shows good coherence but little phase shift at these frequencies between the two stations, which are on opposite sides of the island. These frequencies are quite close to those estimated by Longuet-Higgins from an exact computation of the free oscillations on a hemisphere bounded by meridians and are also close to those calculated for a rectangular model of the Pacific by Rattray & Charnell (1966).

The peaks at 0.50 and 0.73 c/d, however, have frequencies too high to be normal modes of the basin as a whole. Besides, the sea-level variations at the two locations are out of phase at these frequencies. Therefore, they are more likely to be local effects. The peak at 0.73 c/d, the inertial frequency at this latitude, is suggested to represent wave motions similar to Kelvin waves progressing around the island in a clockwise fashion. At 0.50 c/d, we may be seeing an effect of the sloping bathymetry in supporting topographic Rossby waves, which also travel around the island (or perhaps the whole Hawaiian Ridge).

The resonant trapping of waves of period longer than a half-pendulum day by axisymmetric islands has been predicted by Longuet-Higgins (1969, 1970). He considers two types of wave motion: (1) a Kelvin-type wave near an island with vertical

sides and (2) a shelf-type wave near a vertical-sided island surrounded by a sloping shelf. The Kelvin-type wave is similar to an ordinary Kelvin wave in form in that motion is mostly parallel to the shoreline, the dispersion relation reducing to that of the Kelvin wave as the island becomes large compared with the distance the wave travels in a half-pendulum day. The shelf-type wave is supported by sloping bathymetry and the orbital velocities mostly horizontal, so that Longuet-Higgins (1970) assumed the absence of horizontal divergence in his calculations. Frequencies of resonance were calculated for various modes of both types of waves.

In order to see if the predicted resonance phenomena could be realized for these waves, to verify the predicted values of the resonant frequencies, and to assess the effects of finite amplitude of motion, a series of model experiments was undertaken using a rotating basin. The steady currents generated by these wave motions are also of interest.

Model studies of long-period waves supported by bathymetric features have been reported by Phillips (1965), Ibbetson & Phillips (1967), Holton (1971), Caldwell & Longuet-Higgins (1971) and Caldwell, Cutchin & Longuet-Higgins (1972). Phillips calculated and experimentally verified the dispersion relation for waves in a rotating annulus with a flat bottom and a parabolic free surface. Holton calculated resonant frequencies for waves travelling round an annulus with depth varying linearly with radial distance and produced waves travelling at the proper phase speed, but he did not demonstrate resonant amplification of these waves. His photographs of surface motion are strikingly similar to the ones to be shown in the present paper. Caldwell & Longuet-Higgins verified the dispersion relation for 'double-Kelvin' waves and Caldwell *et al.* did the same for waves on an exponential shelf, but in neither case was resonance observed.

In this paper: § 2 contains a sketch of the theory; § 3, an outline of experimental procedures; § 4, results for the Kelvin-type waves; § 5, results for the shelf-type waves and some discussion of reasons why the observed resonant frequencies differ from those predicted. Section 6 shows the effect of varying the amplitude of the excitation, and § 7, the effect of changing horizontal scale, in both cases for the self-type waves. Smaller-scale motions are discussed in § 8 and a summary (§ 9) concludes.

2. THEORY

(a) *Kelvin-type waves (Longuet-Higgins 1969)*

Near a circular, vertical-sided island of radius a lying in a rotating ocean of constant depth, h , the surface elevation ζ is assumed to obey the shallow water equation

$$\left(\nabla^2 + \frac{\sigma^2 - f^2}{gh}\right)\zeta = 0, \quad (2.1)$$

where ∇^2 is the horizontal Laplacian; σ , the angular frequency ($\zeta \propto \exp(-i\sigma t)$) and f and g denote the Coriolis parameter and the acceleration of gravity, respectively. For $\sigma^2 \leq f^2$, solutions of the form $\zeta = K_n(kr) \exp[i(n\theta - \sigma t)]$ represent a trapped

motion, if $k^2 = (f^2 - \sigma^2)/gh$ and if the boundary condition of zero radial velocity at $r = a$ is satisfied. These latter two conditions specify the values of k for which solutions exist at a given value of σ/f . It turns out that only negative values of σ/f are allowable, and that the parameter upon which the value of σ/f depends is $\epsilon \simeq a^2 f^2 / gh$, which we interpret as the square of the ratio of the island radius to the distance a wave travels in a half-pendulum day. If ϵ is large enough that the waves travel only a bit of the perimeter in a half-pendulum day, they reduce to Kelvin waves travelling clockwise around the island in the northern hemisphere.

The resonant frequencies are always less than or equal to f . If $\epsilon < 2$, only the lowest mode can be trapped, and for $\epsilon < 0.1$ its frequency is f , the frequency decreasing with increasing ϵ . For Oahu, $\epsilon \simeq 0.001$, so the frequency of the trapped mode is f . Thus the peak in the tidal records may be ascribed to such a mode, particularly since the phase shift between the two sides of the island is nearly 180° , as would be expected for this mode. This situation would hold for almost any island; only one so large that f would vary greatly over its extent, a factor not considered in the calculations, would be large enough for the period to be longer. However, similar trapping would be expected for baroclinic modes, and since the wave speed is slower, if we use the interpretation of ϵ as the square of the number of half-pendulum days it would take a wave to travel the distance a , the island radius, then ϵ for the internal wave would be larger, by a factor $\rho/\Delta\rho$, $\Delta\rho$ being the change in density ρ across some horizontal surface. Thus for baroclinic modes ϵ could be large enough for a more complex modal structure to be observed.

The relation between resonant frequency and ϵ calculated by Longuet-Higgins is reproduced, with our experimental points, later in this paper (figure 6).

(b) *Shelf-type waves (Longuet-Higgins 1970)*

Here a 'skirt' of radius b is added to the island and the depth variation in the region $a \leq r \leq b$ is given by $h_1(r/a)^\alpha$, h_1 being the depth at the island perimeter. The depth for $r \leq b$ is considered constant, and f is constant. If the horizontal divergence is neglected and shallow water theory assumed, the stream function ψ must satisfy the equation

$$\frac{\partial}{\partial t} \left[\nabla \cdot \left(\frac{1}{h} \nabla \psi \right) \right] - f \cdot \left[\nabla \left(\frac{1}{h} \right) \times \nabla \psi \right] = 0, \tag{2.2}$$

the depth h taking the appropriate form in the different regions. A solution with time and azimuthal variations given by $\exp[i(n\theta - \sigma t)]$ is assumed. The radial velocity is taken to be zero at $r = a$, and matching conditions are imposed at $r = b$ to the solutions on the slope and in the surrounding ocean, to derive equations relating σ/f , n , α and b/a

$$\left. \begin{aligned} \xi' \cot \xi' &= - \left(n + \frac{1}{2} \alpha \right) \ln \left(\frac{b}{a} \right), \\ \xi' &= \ln \left(\frac{b}{a} \right) \cdot \left[\frac{n\alpha}{(-\sigma/f)} - n^2 - \frac{\alpha^2}{4} \right]^{\frac{1}{2}}. \end{aligned} \right\} \tag{2.3}$$

The equations have a series of solutions corresponding to the various branches of the cotangent function. An example of solutions for σ/f as a function of n for specified values of b/a and α is shown as figure 1. Principal values of the cotangent function have been used, so we call this the first mode, $m = 1$. If the second value of the cotangent is used then we say $m = 2$.

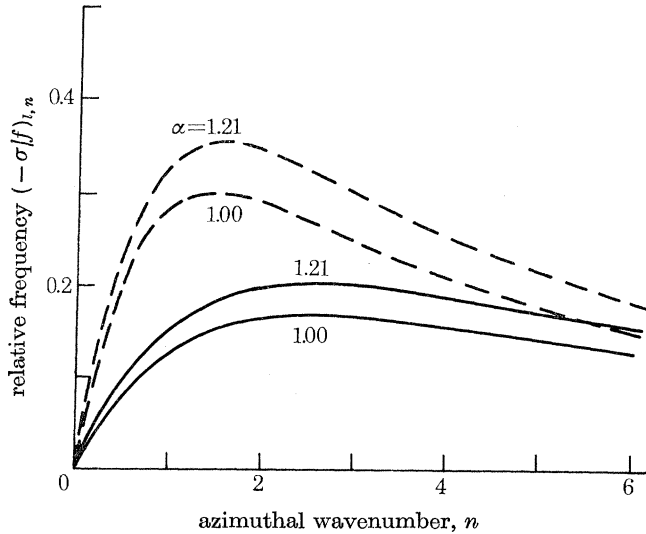


FIGURE 1. Theoretical dispersion curves relating relative frequency, $(-\sigma/f)$, and azimuthal wavenumber, n , for first order radial modes ($m = 1$). Island diameter: ---, 15.4 cm (6.05 in), $b/a = 4.76$; —, 32.4 cm (12.75 in), $b/a = 2.26$.

This dispersion relation is very similar to that for shelf waves on a straight coast, as expected. Resonance occurs when n is an integer, so that an integral number of waves just fit around the island. For any given geometry, specified by α and b/a , these are then a double infinity of resonant modes, specified by (m, n) .

A look at figure 1 shows that the resonant frequencies for the various n are close together, and that modes with higher n may have either higher or lower frequency than the $(1, 1)$ mode. It is possible also for modes of two different wavenumbers to be resonant at the same frequency. If the dissipation is such that the widths of two resonance peaks are comparable to their separation in frequency, the peaks may be indistinguishable.

As we shall see, the flow has the appearance of a cell-like current pattern, the pattern rotating about the island in the clockwise direction. The number of cells in the azimuthal direction is $2n$, and the number in the radial direction is m , for a total of $2mn$ cells in the (m, n) mode.

3. EXPERIMENTAL PROCEDURE

(a) *Physical configuration*

The experimental apparatus consists of a circular basin mounted on a rotating turntable, and is similar to that described by Caldwell & Longuet-Higgins (1971). The turntable is driven by a synchronous motor and continuously variable transmission by means of a timing belt. The bottom of the basin is cast in epoxy resin in a parabolic form, resulting in uniform water depth parallel to the axis of rotation when

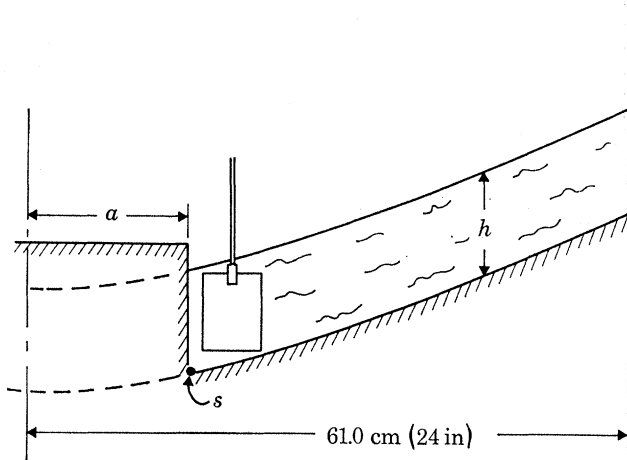


FIGURE 2. Axial half-section of rotating basin as used in Kelvin-type wave studies. Symbols: a , island radius; h , water depth measured parallel to the axis of rotation; s , radial position of sensors relative to island model. (Two sensors are separated by 60° , being located at azimuthal positions 120° and 180° clockwise from the paddle as seen from above.) The axis of rotation is on the left and the paddle oscillation is perpendicular to the plane of the figure.

the basin is rotating (counter-clockwise, as viewed from above) at a constant design speed of $\Omega/2\pi = 0.5$ rev/s. The 2.00 s period of rotation, measured by means of a microswitch actuated during each revolution by a projection on the turntable, varies by less than 0.1 %. The outer wall of the basin has a radius of 61 cm. Electrical power and signals are transmitted to and from the rotating basin through a set of mechanical slip rings. The top of the basin is covered with a sheet of clear acrylic plastic 0.95 cm thick.

The wave generator system consists of a single paddle suspended vertically from an oscillating horizontal drive shaft driven by a small d.c. motor through a gear reduction unit. The requirement of high stability over a wide range of driving frequencies under variable load conditions resulted in the development of a precision speed controller (Wilcox, Eide & Caldwell 1974) for the d.c. motor. This device maintains the motor rotation speed constant to within 0.1 % or less for the entire range of driving frequencies used in this study.

(i) *Kelvin-type waves*

For the study of Kelvin-type waves, a circular cylindrical island of radius a is placed at the centre of the rotating basin (figure 2). The waves are generated by a rectangular paddle 8.1 cm wide and 10.2 cm in height, which oscillates tangentially at the perimeter of the island. The length of the paddle arm measured from the centre of the paddle to the axis of the paddle drive shaft is 33.6 cm. The amplitude of paddle oscillation is 6.0° measured at the axis of the paddle drive shaft.

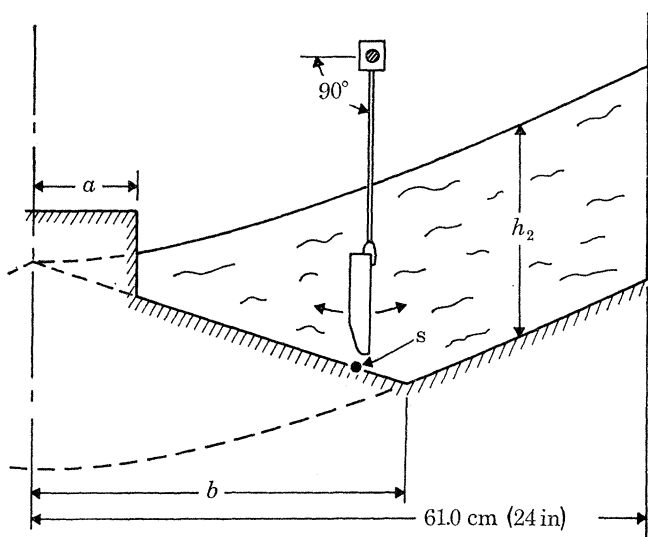


FIGURE 3. Axial half-section of rotating basin as used in shelf-type wave studies. Symbols: a , island radius; b , shelf radius 36.6 cm; h_2 , deep-water depth measured parallel to axis of rotation 20.3 cm; s , radial position of sensors relative to island model (sensors are located azimuthally at 90° , 180° , and 270° clockwise from the paddle as seen from above). The paddle oscillates in the plane of the figure as shown. The axis of rotation of the basin is on the left.

A differential pressure transducer (Statham Model PM5TC; ± 0.15 p.s.i.d. range) mounted atop the island is connected to two pressure sensing ports ('sensors') located at the base of the island's perimeter on the side opposite the paddle, separated azimuthally by 60° . The depth of the water, h , is varied to allow the response of the system as a function of wave generator frequency to be studied at different values of the parameter af/\sqrt{gh} for each island.

(ii) *Shelf-type waves*

For the study of shelf-type waves a circular cylindrical island of radius a surrounded by a sloping shelf or 'skirt' of radius $b = 36.6$ cm is placed at the centre of the rotating basin (figure 3). The waves are generated by a large rectangular curved paddle 39.6 cm wide, 9.9 cm in height with a radius of curvature of approximately 33 cm. The paddle oscillates radially above the perimeter of the sloping shelf. The

length of the paddle arm measured from the centre of the paddle to the axis of the paddle drive shaft is 26 cm. The amplitude of paddle oscillation generally used is 6.5° measured at the axis of the paddle drive shaft. The effects of using larger and smaller paddle amplitudes are discussed later.

Three pressure-sensing ports are located on the sloping shelf near its perimeter at azimuthal positions of 90° , 180° and 270° relative to the paddle. The response of the

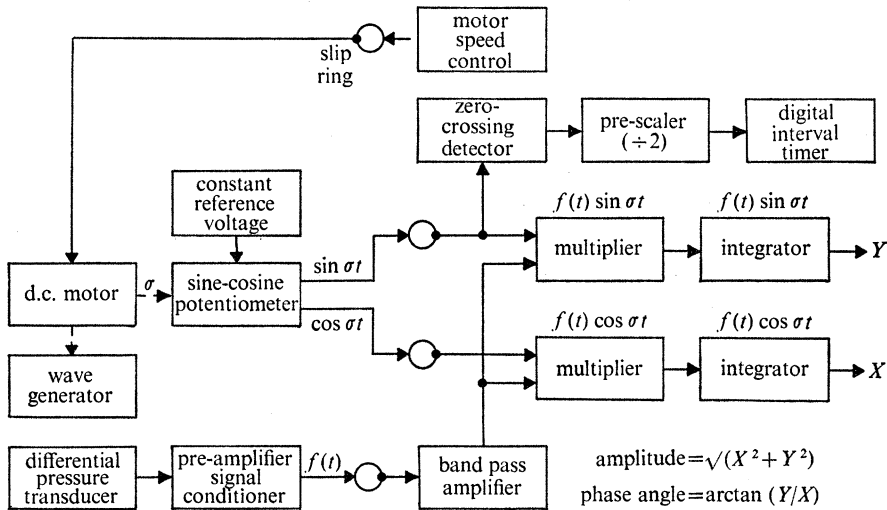


FIGURE 4. Block diagram of electronics.

system as a function of wave generator frequency is then measured twice for each island studied, using the differential pressure transducer connected to sensors separated by first 90° , then by 180° . A deep-water depth of $h_2 = 20.3$ cm is used for all islands investigated.

(b) *Quantitative measurements*

A functional block diagram of the electronics is shown in figure 4. The detection and measurement of relative wave amplitudes in the region surrounding the central island is accomplished through the use of the differential pressure transducer. The transducer consists of two chambers separated by a thin diaphragm. Each chamber is connected by plastic tubing to one of the sensing ports located at or near the perimeter of the island models described above. Mounted on either side of the diaphragm are electrical resistance strain which in turn comprise the arms of a Wheatstone bridge circuit. The output voltage of the bridge circuit provides a time-dependent signal which is amplified and filtered before being transmitted through a set of slip rings to a band-pass amplifier and high- Q electromechanical synchronous filter. The reference voltages used by the synchronous filter are generated in quadrature mechanically by means of a 360° precision sine-cosine potentiometer which is driven at frequency σ directly by the wave generator motor through a

timing belt. The input signal, $f(t)$, is then multiplied by $\sin \sigma t$ and $\cos \phi t$ in the dual channels of the synchronous filter. The output of each multiplier passes through a final integrator where the signal is continuously averaged over an r.c. time constant of 100 s. The averaged output voltages are corrected for d.c. offsets in the final stage of the electronics and recorded as rectilinear coordinates, $x = \overline{f(t) \cos \sigma t}$ and $y = \overline{f(t) \sin \sigma t}$ as a function of σ . The relative amplitude is computed as the square root of the sum of the squares of x and y ; the phase angle is given by $\theta = \arctan (y/x)$. Both are then plotted as functions of the relative frequency, $(-\sigma/f)$, for each island-sensor combination. In the case of the shelf-type waves, comparison of relative heights of the resonance peaks for the 90° and 180° sensors provides a means of tentatively identifying certain azimuthal modes. For example, the second order azimuthal modes ($n = 2$) exhibit a large resonance peak with 90° sensors, but little or no peak with 180° sensors.

The period of the wave generator is measured by a digital interval timer connected through a bi-stable pre-scaler to a zero-crossing detector which monitors the sine reference voltage.

(c) *Visual observations*

Surface currents are recorded by means of streak photographs. The water in the basin is dyed black and the surface sprinkled lightly with finely divided aluminium powder. Any horizontal motion of the aluminium particles on the surface (relative to the rotating frame of reference) during the exposure will result in streaks in the photographic image. The time-lapse time exposures are made by a remotely controlled 16 mm motion picture camera mounted atop a tower attached to the rotating basin. The electronically controlled camera shutter allows remote independent adjustment of both exposure time and lapse time between successive exposures.

For the particular combination of camera lens, camera-to-subject distance and film used in this work, the quality of the streak photographs was studied as a function of exposure time. In the case of the Kelvin-type waves the optimum exposure times were approximately one-half the paddle period. For shelf-type waves the optimum exposures were approximately 30 % of the paddle period.

Determinations of azimuthal currents were made by measurement of streak lengths in the photographs. Perspective correction was made for variation in the photographic image size due to curvature of the parabolic free surface.

4. RESULTS FOR KELVIN-TYPE WAVES

With the tank set up to observe Kelvin waves (figure 2), the magnitude and phase of the signal seen by the differential pressure transducer looking at pressure sensing ports located 60° apart on the island perimeter is shown in figure 5. In this case response reaches a peak at $\sigma/f = -0.72$, and the phase changes by roughly 180° across the peak. The Q of this peak, defined as the centre frequency divided by the width measured at an amplitude of 0.5 times the peak amplitude, is 8.2.

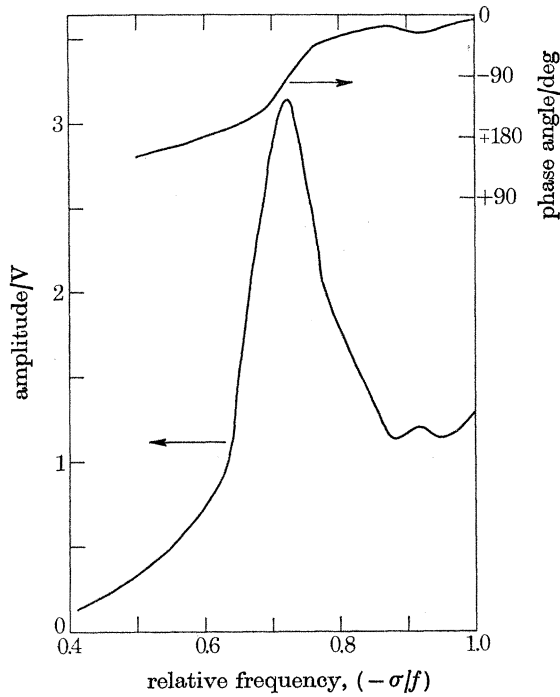


FIGURE 5. Typical experimental response curves (60° sensors) for Kelvin-type waves. Island: diameter 32.4 cm (12.75 in); radius, a , 16.2 cm (6.38 in); water depth, h , 13.3 cm (5.25 in); $\sigma f/\sqrt{gh} = 0.89$.

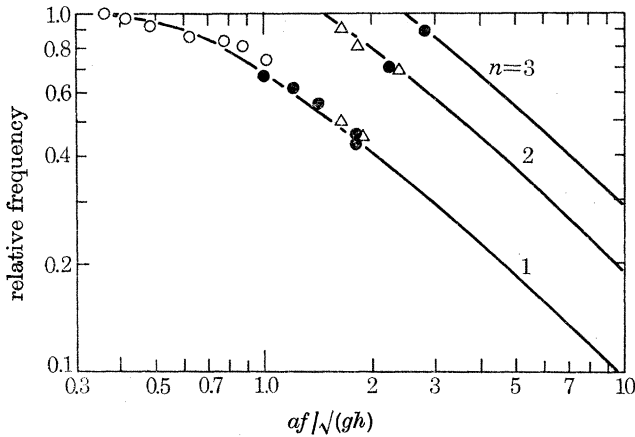


FIGURE 6. Theoretical curves and experimental points relating relative frequency, $(-\sigma/f)$, and the parameter af/\sqrt{gh} for the three lowest azimuthal wavenumbers, $n = 1, 2, 3$. Island radius, a : \circ , 7.1 cm (2.8 in); \bullet , 16.2 cm (6.38 in); \triangle , 30.4 cm (12.0 in).

The parameter $\epsilon^{\frac{1}{2}} \simeq af/\sqrt{gh}$ upon which the resonant frequency depends can be varied, for constant f , by changing the water depth or by using a different island. In figure 6 the resonant frequencies for three islands are shown plotted against $\epsilon^{\frac{1}{2}}$, together with the theoretical curves. Larger values of $\epsilon^{\frac{1}{2}}$ are hard to achieve because a is limited by the size of the rotating basin and the depth must be kept much larger than the Ekman layer depth to avoid large damping.

Photographs of the aluminium-powder-covered water surface (figures 7 and 8, plates 3 and 4) are a bit difficult to interpret. Unlike the shelf-type wave, the Kelvin-type has no return current, i.e. the motion is tangential only and no cells are to be seen. We must look for tangential motion, strongest near the island, which for the lowest mode (shown here) has two regions of intensity, 180° apart, separated by quiet spots. A sequence must be examined to see if the active spots move in a clockwise direction around the island. Close examination of the figures reveals these features.

An order-of-magnitude estimate of Q from the bottom damping (Caldwell & Longuet-Higgins 1971), $Q = (\frac{1}{2}\pi)(h/\delta)(\sigma/f)$, yields $Q = 26$ (Here δ is the Ekman layer depth $(2\nu/f)^{\frac{1}{2}}$). The damping from the island walls will be large because the velocity is highest there, so the experimentally determined number is not unreasonable.

Thus good agreement with the theoretical calculations is found for the Kelvin-type wave.

5. RESULTS FOR SHELF-TYPE WAVES

With the sloping shelf (figure 3) waves of quite a different appearance are seen (figures 9–11, plates 5–7). Now the wave motion appears as a moving, circulating current system. The resemblance to Holton's (1971) photographs is striking. The direction of flow can be inferred from the pictures because the steady flow near the island is always clockwise. This flow reinforces the 'lows', but interferes with the 'highs'.

The response to excitation by the paddle (figure 12) is more complex than for the Kelvin-type waves. With the value of b/a appropriate to this figure the calculation predicts waves of five different azimuthal wavenumbers resonant in the frequency range $0.20 < |\sigma/f| < 0.35$. The paddle is 39.6 cm wide, wide enough to favour the lower modes. In this case we seem to have excited principally the (1, 1) mode at $\sigma/f = -0.18$ and the (1, 2) mode at $\sigma/f = -0.26$. The peak at -0.18 appears much higher when the pressure sensing ports are 180° apart than when they are 90° apart. At -0.26 on the other hand there is no distinct peak for 180° sensors but a good peak for 90° sensors. (A second order azimuthal mode should be invisible to 180° sensors, except for the degree to which the motion is less on one side of the island because of damping.) The phase shift between $\sigma/f = -0.10$ and $\sigma/f = -0.30$ is about 360° , as might be expected if two modes are excited between these frequencies.

To make sure that the observed peaks were not a function of the method of

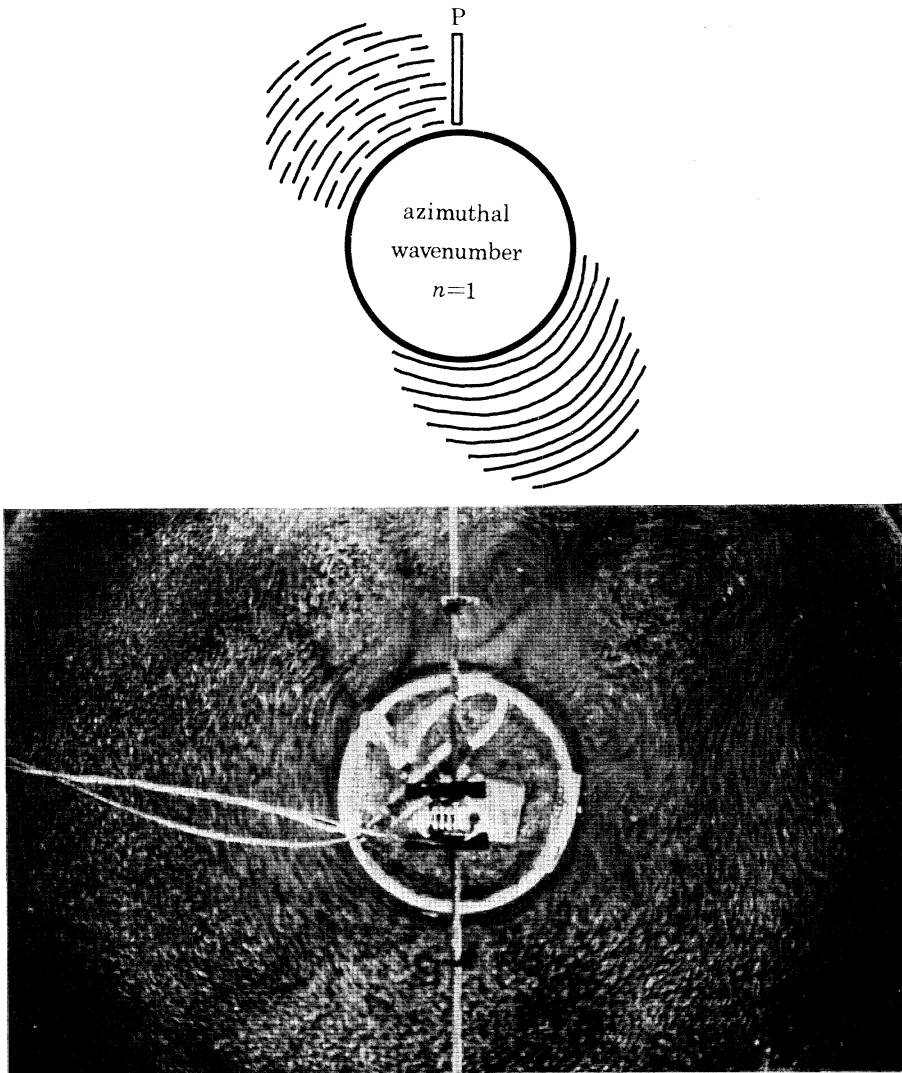


FIGURE 7. Streak photograph of Kelvin-type wave. The $n = 1$ mode is visible as azimuthal streaks at the lower right and upper left of the island (See interpretive diagram above photograph.). The paddle, P, is at the top in the photograph. Kelvin-type waves move clockwise around the island; other features are stationary. Island radius $a = 16.2$ cm; water depth $h = 13.3$ cm; $\alpha f / \sqrt{gh} = 0.89$; $\sigma / f = -0.725$; exposure time = 0.69 s; Kodak Plus-X Reversal film (7276).

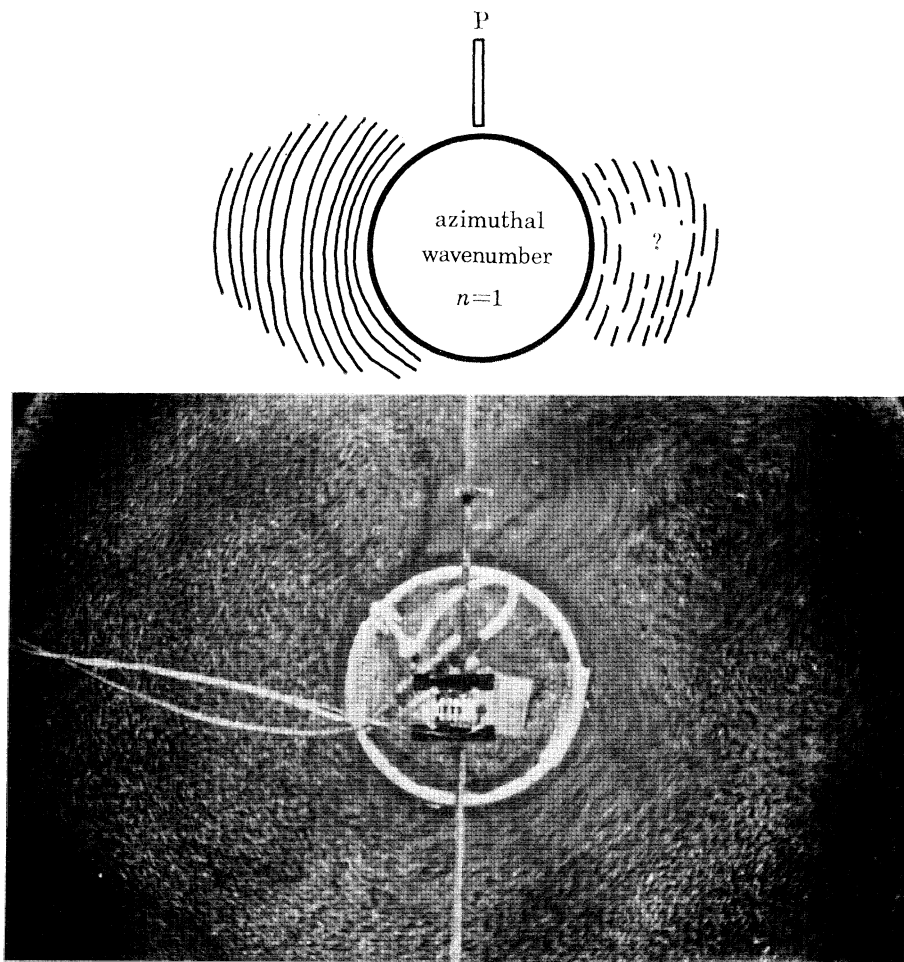


FIGURE 8. Kelvin-type wave. Same as figure 6, except photograph taken 1.3 wave periods (1.79 s) later. Azimuthal streaks associated with the $n = 1$ mode are clearly visible to the left of the island perimeter.

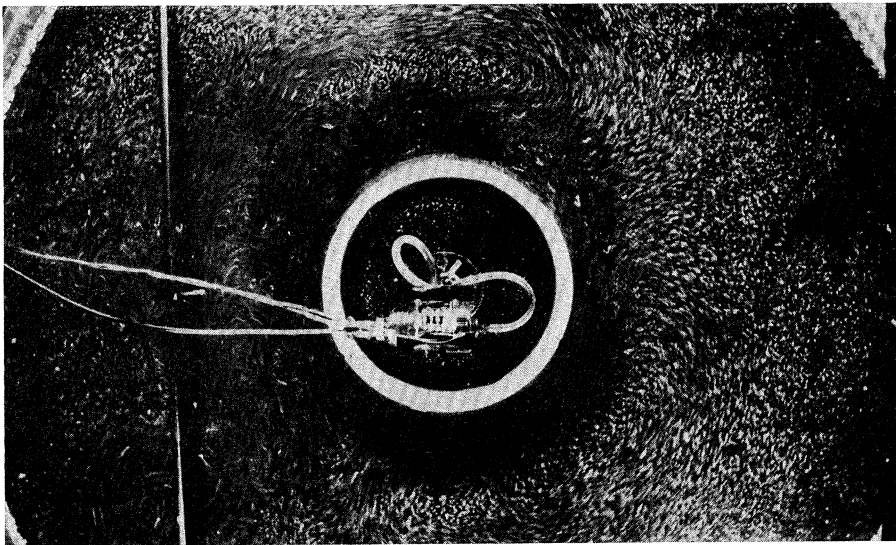
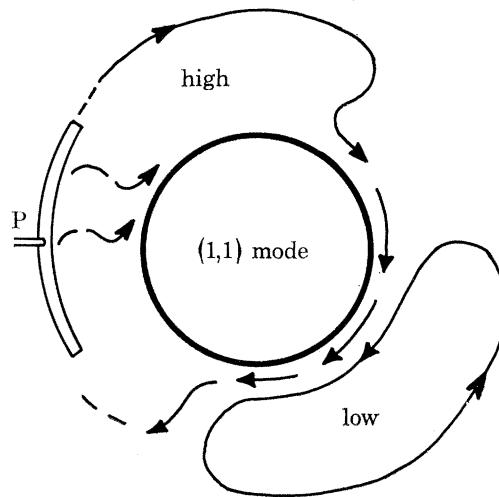


FIGURE 9. Streak photograph of $(1, 1)$ mode shelf-type wave. The surface flow patterns associated with the 'high' and 'low' regions of the $(m, n) = (1, 1)$ mode are seen (refer to interpretive diagram). Curved paddle, P, is to the left of the island. Waves move clockwise around the island-shelf model. Island radius $a = 16.2$ cm; shelf radius $b = 36.6$ cm; $b/a = 2.26$; deep-water depth $h_2 = 20.3$ cm; relative frequency $\sigma/f = -0.102$; exposure time = 2.94 s.

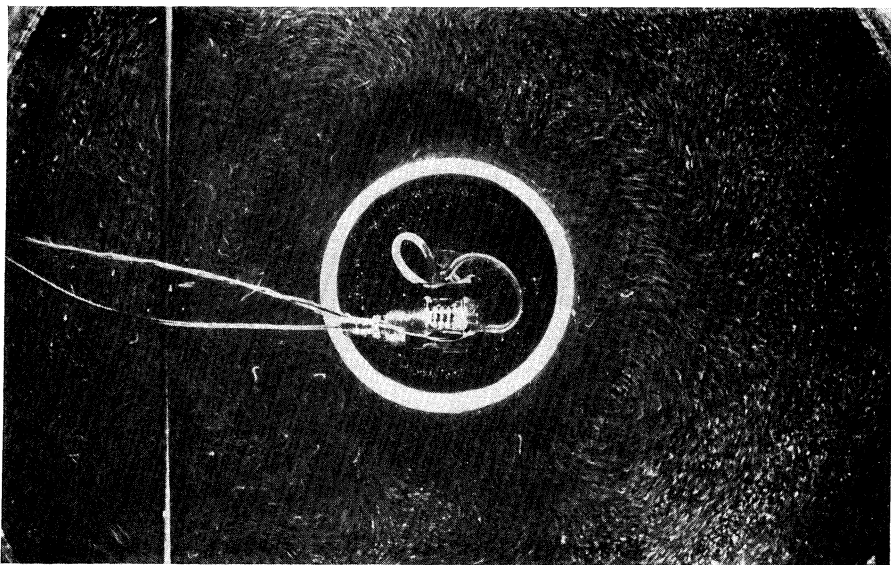
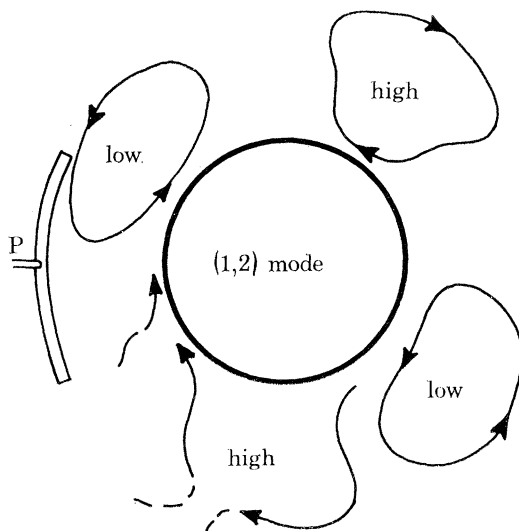


FIGURE 10. Streak photograph of (1, 2) mode shelf-type wave. Same configuration as figure 9, except $\sigma/f = -0.164$ and exposure time = 1.80 s. The small stationary features visible near the paddle at the far left are associated with turbulence generated at the ends of the paddle and do not propagate around the island.

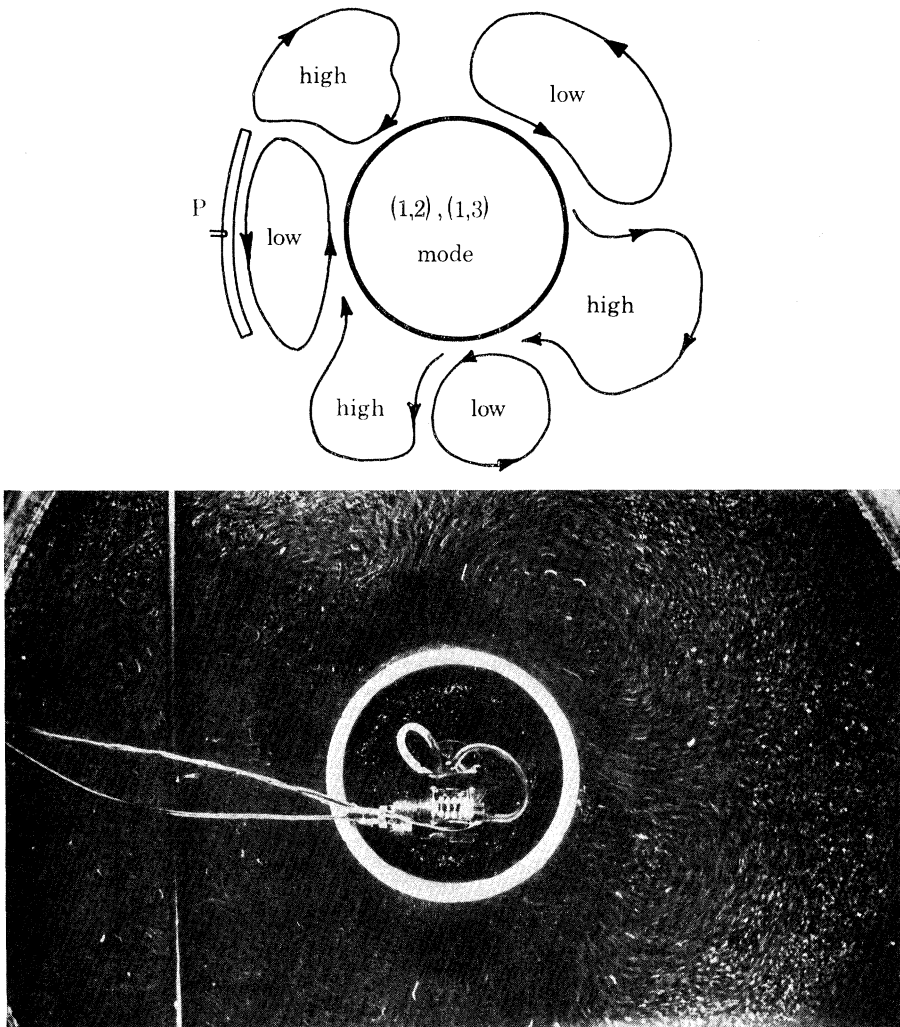


FIGURE 11. Streak photograph of (1, 2) and (1, 3) mode shelf-type waves. Theoretical dispersion curves (figure 1, lower curves) suggest the possibility of (1, 2) and (1, 3) modes with the same frequency but with group velocities of opposite sign. Spacing of cells clockwise from the paddle suggests a (1, 2) mode; the spacing counter-clockwise from the paddle is that of a (1, 3) mode. Parameters: $a = 16.2$ cm; $b = 36.6$ cm; $b/a = 2.26$; $h_2 = 20.3$ cm; $\sigma/f = -0.179$; exposure time = 1.68 s.

generation, a similar response plot was obtained by using a plunger to generate the waves (figure 13). Comparison with paddle-generated response plots shows no significant difference in the frequencies at which the peaks appear.

The peak at $\sigma/f = -0.42$ is not associated with the island but with the basin as a whole. Precisely this value is predicted theoretically for free oscillations of a horizontal circular sheet of water of uniform depth rotating about a central vertical axis

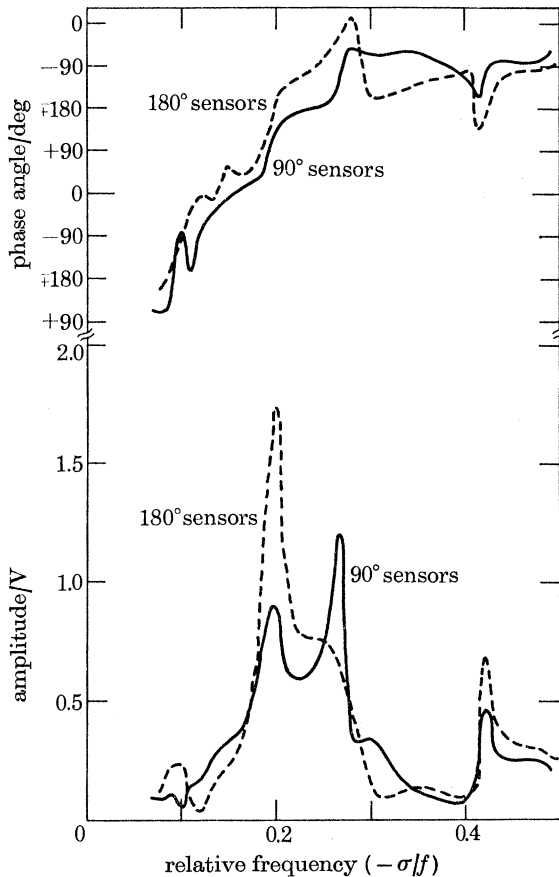


FIGURE 12. Typical experimental response curves for shelf-type waves. Peak at $(-\sigma/f) = 0.199$ is (1, 1) mode; peak at $(-\sigma/f) = 0.267$ is (1, 2) mode; peak at $(-\sigma/f) = 0.102$ is (2, 3) mode; peak at $(-\sigma/f) = 0.42$ is described in figure 13. Island: diameter 15.4 cm (6.05 in); radius, a , 7.70 cm (3.03 in); $b/a = 4.76$.

(Lamb 1932), where the depth is taken to be an average obtained by dividing the total volume of water by the total free surface area. This frequency corresponds to the first order azimuthal mode with a single nodal line across the diameter of the basin. This interpretation is supported by the relatively larger-amplitude resonance peak at $\sigma/f = -0.42$ for the 180° sensors as compared to that for the 90° sensors (figure 12). Other similar modes have higher resonant frequencies, $\sigma/f = -0.8$ and $\sigma/f = +1.73$ being the next smallest, so are not seen in our data.

The identification of these peaks with specific modes was further confirmed by examination of the streak photographs taken while the paddle was oscillating at the peak frequency. In figure 9 a (1, 1) mode is apparent and in figure 10 a (1, 2) mode appears, as expected from the measured responses.

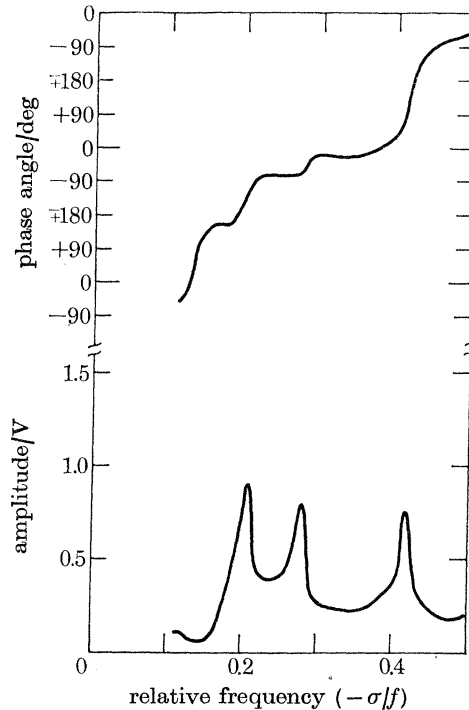


FIGURE 13. Experimental response curves for plunger-driven shelf-type waves. (90° sensors). Configuration same as for figure 14, except that waves are generated by means of an oscillating weighted circular-cylindrical plunger (diameter = 10.5 cm; vertical travel = 2.2 cm). Island: diameter 15.4 cm (6.05 in); radius, a , 7.70 cm (3.03 in); $b/a = 4.76$.

As previously mentioned, it is possible to have two modes resonant at indistinguishable frequencies, separated by less than the peak widths. An example might be shown in figure 11. Here the waves clockwise from the paddle appear larger in extent than those counter clockwise from it. (The patterns appear to travel clockwise with similar phase velocities.) This might be explicable in terms of the group velocities, which must be opposite for two modes resonant at the same frequency. The group velocity of the shorter waves would be counter-clockwise, hence they might be damped sufficiently by the time they have travelled around the island to allow the long waves, with clockwise group velocity, to predominate there.

The observed values of Q for the peaks are about 10, somewhat lower than expected from viscous damping.

The resonant frequencies determined for several values of α are plotted against b/a for each mode in figures 14 and 15, together with calculated curves. The value

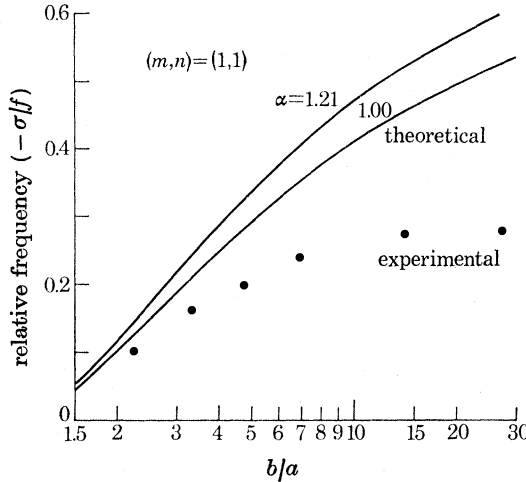


FIGURE 14. Theoretical curves and experimental points relating relative frequency, $(-\sigma/f)$, and parameter b/a for the $(m, n) = (1, 1)$ mode shelf-type wave. The experimental points shown have been verified photographically.

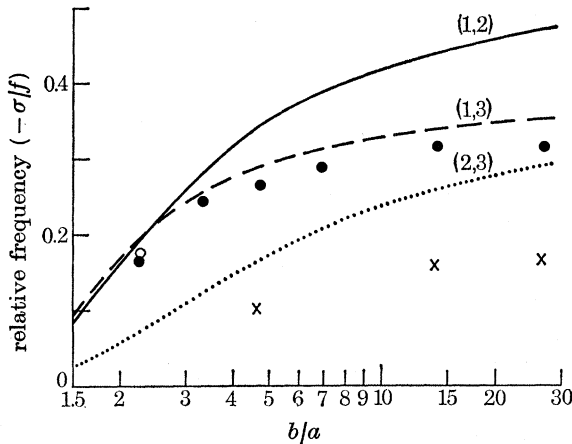


FIGURE 15. Theoretical curves and experimental points relating relative frequency, $(-\sigma/f)$, and parameter b/a for the $(m, n) = (1, 2)$ mode (○) shelf-type wave, and also the $(1, 3)$ (●) and $(2, 3)$ (×) modes.

$\alpha = 1.21$ is the value of α obtained when the depth variation in the shelf region is approximated by the form r^α , taking into account the parabolic shape of the free surface.

While the resonant frequencies are of the same order as predicted, and vary with b/a in the expected manner, the measured frequencies are consistently lower than predicted, particularly for the $(1, 1)$ mode, the discrepancy growing more serious at the larger values of b/a (smaller islands).

Why these discrepancies?

(1) *Errors in the form of the island and slope.* As seen in the figures (e.g. figure 14) a change in α of 20 % does not change σ/f very much. The errors in making the model could not be nearly this great.

(2) *Divergence.* The horizontal divergence of the currents was ignored in the calculations. A parameter $\tilde{\omega} \simeq Wf^2/gh'$ was used by Caldwell & Longuet-Higgins (1971) to express its effect. For waves on an exponential shelf it was found that including the divergence in the calculation lowered the value of $|\sigma/f|$ calculated for a given wavenumber. Here $2W$ is the shelf width and h' its slope. In the terms of this paper $\tilde{\omega} = b(b-a)f^2/(2gh_2)$ which can be rewritten as $(b^2f^2/2gh_2) \cdot (1 - (b/a)^{-1})$. Only b/a changes in our experiments, so numerically $\tilde{\omega} = 1.32 (1 - (b/a)^{-1})$. For $\tilde{\omega} = 0.29$ a 20 % reduction in $|\sigma/f|$ for the first mode was found by Caldwell & Longuet-Higgins, less for higher modes. The discrepancies observed are reductions of order 50 %, less for the higher modes, while $\tilde{\omega}$ varies from 0.66 at $b/a = 2$ to 1.3 at $b/a = 30$. Thus the effect of horizontal divergence is a good candidate for the cause of the reduction in frequency. In § 7 some pertinent experiments will be described.

(3) *Effect of the outside wall of the tank.* The imposition of boundary conditions at the exterior was also found by Caldwell & Longuet-Higgins to lower the frequencies, for the lower wavenumbers particularly, but only by a few percent for waves somewhat closer to the boundaries than these. So the exterior boundary probably had little effect.

(4) *Failure of shallow-water theory.* In the theoretical calculations, shallow-water theory was assumed, thereby making the assumptions that the bottom slope is small, as well as the relative change of depth in a horizontal distance of a wavelength. Neither condition is well satisfied in these experiments. Somerville (1972) states that for ordinary gravity waves shallow-water theory applies if $\sigma^2 h/g < \frac{1}{3}$, well satisfied in our case. However, if the gravity wave dispersion relation is used to translate this into a condition on wavelength, h is required to be less than $\frac{1}{16}\lambda$, λ being the wavelength, and this latter condition is not satisfied. So we cannot say whether shallow-water theory applies. Further experiments pertinent to this point will be presented.

(5) *Nonlinear effects.* The motions seen in the photographs clearly manifest nonlinear effects. In a linear system the 'highs' would look the same as the 'lows'. The streaming near the island is also a nonlinear effect. In § 6 the effect of changing the amplitude of excitation is investigated.

(6) *Dissipation.* For the observed Q of 10, a negligible shift in resonant frequency would be expected in the usual sort of resonant system, such as a pendulum or mass on a spring.

6. EFFECTS OF AMPLITUDE VARIATION

Wondering if the discrepancies between calculated and observed resonant frequencies could be caused by finite-amplitude effects, we excited the system with a wide range of amplitudes, still using the same paddle. Response plots and streak

photographs were made as before, together with measurements of the 'streaming' currents. These more-or-less steady currents interact with the wave motions and distort them. In figure 16, plate 8, for which the paddle amplitude was $\frac{8}{3}$ larger than previously, a (1, 4) mode can be discerned by observing the distinct 'lows' separated

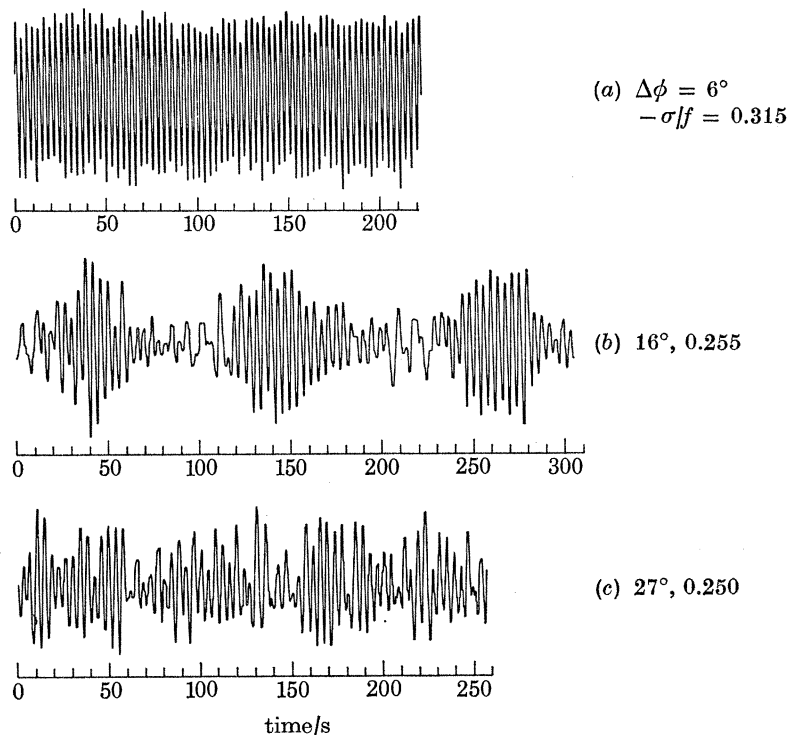


FIGURE 17. Typical transducer signal at resonance as a function of paddle amplitude, $\Delta\phi$.
 (a) $\Delta\phi = 6^\circ$ (normally used); $(-\sigma/f) = 0.315$; (b) $\Delta\phi = 16^\circ$ (note modulation);
 $(-\sigma/f) = 0.255$; (c) $\Delta\phi = 27^\circ$; $(-\sigma/f) = 0.250$. For (a), (b) and (c): $a = 1.33$ cm;
 $b = 36.6$ cm; $b/a = 27.5$; $h_2 = 20.3$ cm.

by 90° , with indistinct 'highs' between. The gyres representing the wave motion appear at a greater distance from the centre island at this amplitude, seemingly forced outwards by the strong streaming.

Could this effect change the resonant frequencies?

We tried to make a series of response plots, varying the paddle amplitude, but were frustrated at some amplitudes by a rather odd effect. The averaged signals would not settle down. The amplified signal from the pressure transducer was found to have changed in character (figure 17). With the paddle swinging only in a 6° arc, the signal had the appearance of a fairly steady sinusoid, but with 16° amplitude, the signal becomes severely modulated. At 27° the modulation is not so clear, and the signal itself is less sinusoidal.

Streak photographs at the 16° amplitude reveal gyres travelling very slowly

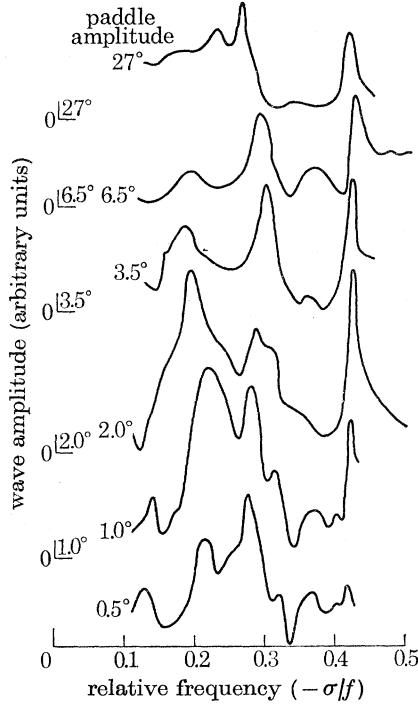


FIGURE 19. Effect of paddle amplitude on response curves for 180-degree sensors. For all curves: $a = 1.33$ cm; $b = 36.6$ cm; $b/a = 27.5$; $h_2 = 20.3$ cm.

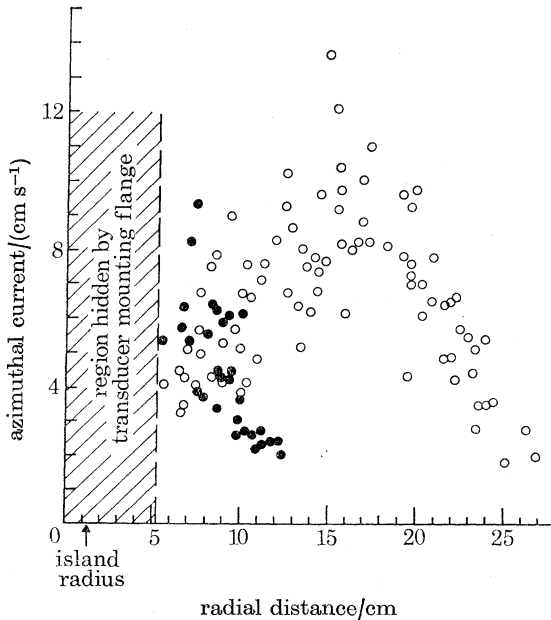


FIGURE 20. Azimuthal surface current as a function of radial distance for paddle amplitude $\Delta\phi = 6.5^\circ$ and $\Delta\phi = 16^\circ$ (●). The experimental points are calculated from perspective-corrected measurements of streak photographs.

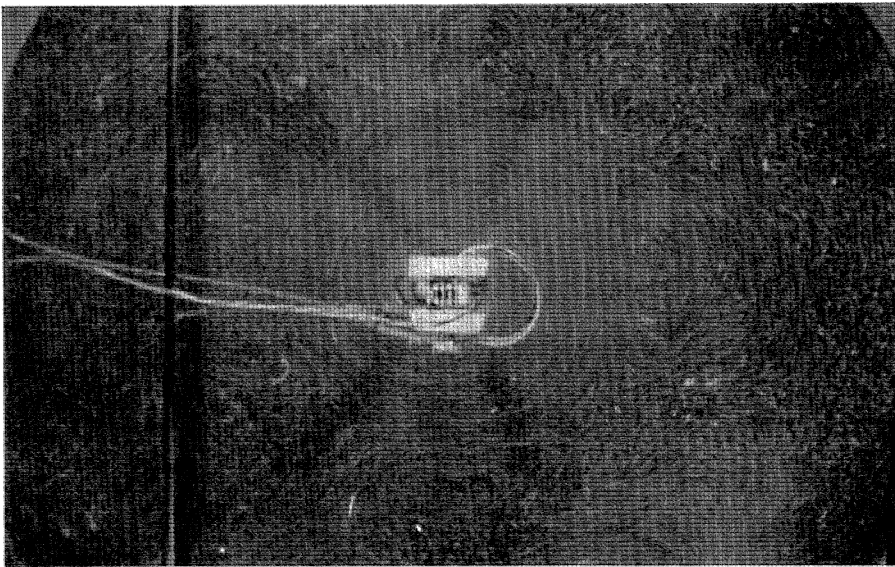
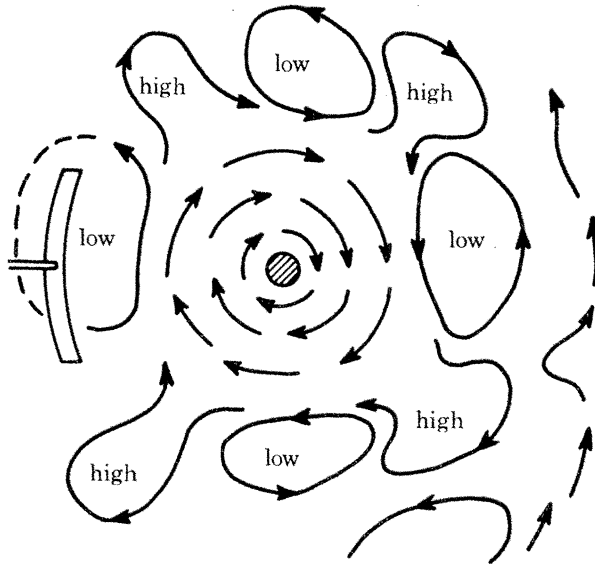


FIGURE 16. Effect of large paddle amplitude. Here the 16-degree paddle amplitude has enhanced the steady clockwise streaming around the island. The orbital gyres of the (1, 4) mode shelf-type wave have been forced radially outward. Parameters: $a = 1.33$ cm; $b = 36.6$ cm; $b/a = 27.5$; $h_2 = 20.3$ cm; $\sigma/f = -0.260$; exposure time = 1.15 s.

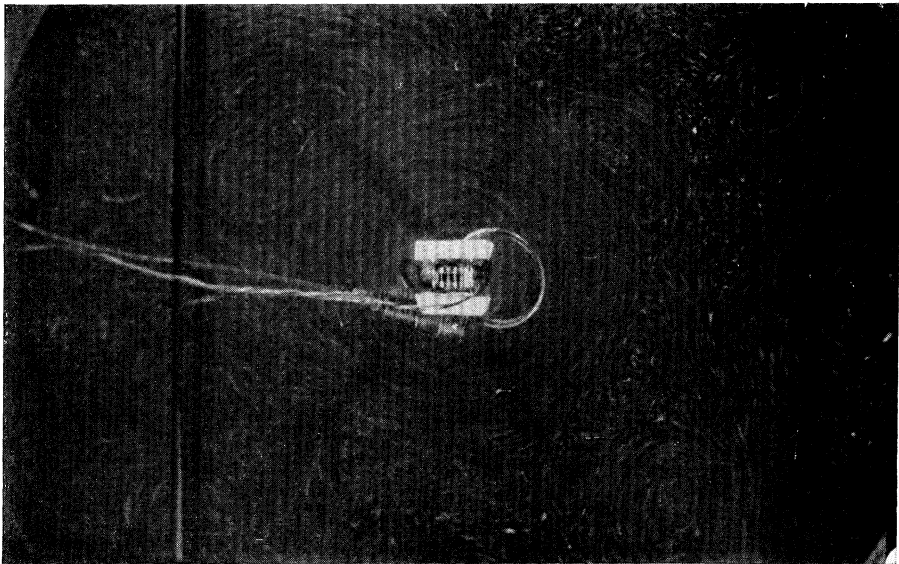
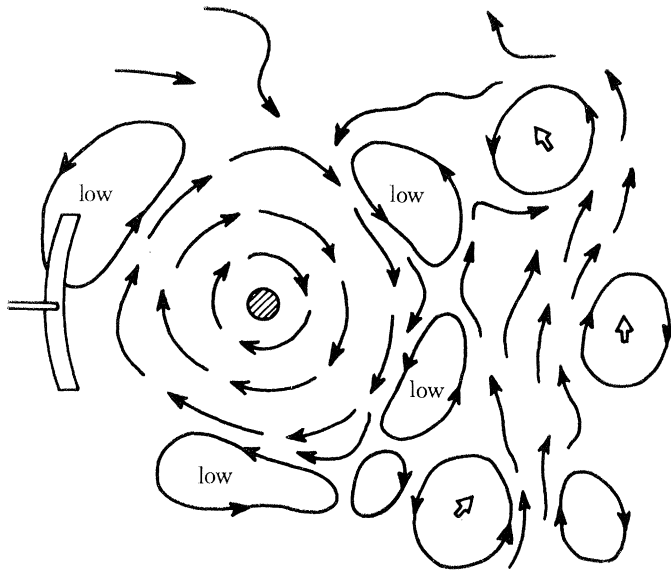


FIGURE 18. Effect of large paddle amplitude. Same configuration as figure 20. Note prominent gyres (3) at far right. These gyres move slowly counter-clockwise (approximately 1 cm/s) around the island, interacting with the shelf-type waves moving clockwise, resulting in modulation of the transducer signal.

counter-clockwise around the outside of the basin (figure 18, plate 9). These evidently interact with the much faster moving wave motions and increase or decrease the wave amplitudes depending on the azimuthal position of the exterior gyres. At 27° amplitude the gyres can still be seen.

Because of this modulation, response plots were obtained only for amplitudes of 6.5° and below, and at 27° (figure 19). The interpretation of these is a bit difficult because the streak photographs do not come out well enough for mode identification at the lower amplitudes. In figure 19, the peak in the 6.5° plot at $(-\sigma/f) = 0.28$ has been definitely identified with a (1, 1) mode. One can follow it down through the different plots, and see that, though the form changes, the centre frequency stays within the range 0.275–0.300, a variation of about 12%. Obviously the amplitude has little effect on the frequencies of the peaks at the lower amplitudes and therefore the paddle amplitude does not appear to be the cause of the discrepancy from the theoretical predictions.

The streaming currents (figure 20) were measured by noting the distance clumps of aluminium powder moved from one frame to another in a sequence of photographs. The increase in current strength and in radial extent of the current as the paddle amplitude is increased is evident.

TABLE 1. COMPARISON OF THEORETICAL AND EXPERIMENTAL VALUES OF RELATIVE FREQUENCY, σ/f , AT RESONANCE FOR SMALL SHELF MODEL ($b = 19.1$ cm; $\alpha = 1.04$; $b/a = 14.4$) AND LARGE SHELF MODEL (USED THROUGHOUT STUDY OF SHELF-TYPE WAVES; $b = 36.6$ cm; $\alpha = 1.21$; $b/a = 27.5$)

(Common parameters: $a = 1.33$ cm; $h_2 = 20.3$ cm. Modes verified photographically.)

shelf radius	mode	theoretical	experimental	difference (%)
$b = 19.1$ cm	(1, 1)	-0.471	-0.330	30
($\alpha = 1.04$)	(1, 2)	-0.389	-0.205	47
$b = 36.6$ cm	(1, 1)	-0.599	-0.280	53
($\alpha = 1.21$)	(1, 2)	-0.475	-0.315	34

7. EFFECT OF CHANGING THE HORIZONTAL SCALE

The divergence parameter depends on b^2 , the square of the total island-plus-shelf radius. If the neglect of the horizontal divergence in the theoretical calculations were the cause of the discrepancies between measured and calculated resonant frequencies, a reduction in b would reduce that discrepancy. Response plots and photographs were made for a model with b half as large. Comparison with theory is shown in table 1. The agreement is neither greatly improved nor worsened with this factor-of-four reduction in divergence parameter.

Any problem with the applicability of shallow water theory would be worsened for the smaller model because of the greater slope. Based on the above results, neither of these effects can be definitely cited as the cause of the discrepancy.

One effect noticed in the course of this procedure was that the peak frequency

depended somewhat on the paddle position. The results given in the table were obtained with the paddle in the same position as for the experiments with the larger island, so that it remained at twice the radius of the edge of the shelf. To get sufficient amplitudes for the photographic identifications, the paddle was moved to the edge of the shelf, and this *reduced* the peak frequency by 12% for the (1, 1) mode.

If the outside wall of the tank exerted a significant influence, the smaller-scale waves on the smaller shelf would be less influenced; the lack of improvement of agreement argues against the significance of this effect, also.

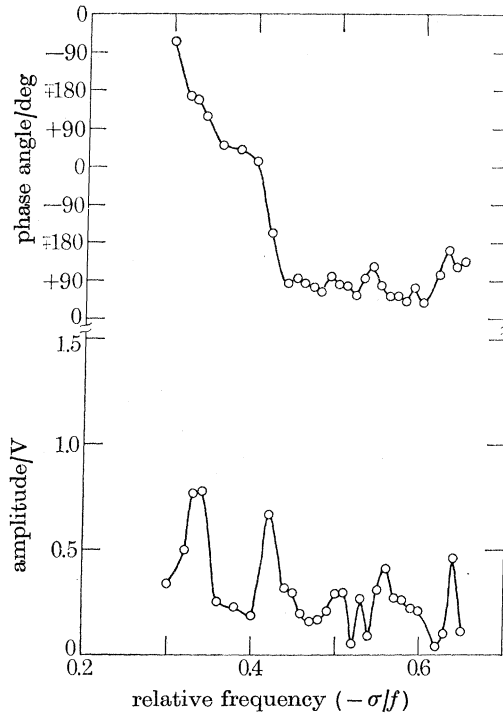


FIGURE 21. High-frequency experimental response plot.

8. SMALLER-SCALE MOTIONS

At frequencies somewhat higher than those at which strong peaks were found, some smaller peaks appeared (figure 21). Photographs show small-scale motions, but modes with high radial wavenumbers would appear at lower frequencies according to the calculations. The peaks are not very high, so perhaps these are just motions somehow favoured by the driving mechanism.

9. CONCLUSIONS

From observations of waves of period longer than a half-pendulum day circulating around cylindrically-symmetrical islands we find

For Kelvin-type waves, prominent resonant peaks at frequencies in excellent agreement with the calculations of Longuet-Higgins (1969).

For shelf-type waves, resonance is demonstrated but the frequencies agree only qualitatively with the calculations of Longuet-Higgins (1970). The variation of the resonant frequencies with the shelf-radius-to-island-radius ratio (b/a) follows the theoretical predictions, but the experimentally determined magnitudes are too small.

Some obvious candidates for the cause of the disagreement in resonant frequency are eliminated; (*a*) errors in model construction, (*b*) influence of the outside wall of the tank, (*c*) nonlinear effects and (*d*) dissipation.

Neither horizontal divergence nor failure of shallow-water theory could be eliminated as the cause of the discrepancy.

At certain amplitudes a modulation of the shelf-type waves by gyres travelling in the opposite sense around the outside of the tank appears.

Smaller-scale motions are seen at frequencies somewhat higher than the larger-scale shelf waves.

The interest of Professor M. S. Longuet-Higgins, F.R.S., generated these experiments. S. D. Wilcox constructed the analog data-processing system, the electronic camera controls and the motor-speed controller. Financial support was furnished by the National Science Foundation under Grant GA-30712.

REFERENCES

- Caldwell, D. R. & Longuet-Higgins, M. S. 1971 The experimental generation of double Kelvin waves. *Proc. R. Soc. Lond. A* **326**, 39–52.
- Caldwell, D. R., Cutchin, D. L. & Longuet-Higgins, M. S. 1972 Some model experiments on continental shelf waves. *J. mar. Res.* **30**, 39–55.
- Holton, J. R. 1971 An experimental study of forced barotropic Rossby waves. *Geophys. Fluid Dyn.* **2**, 323–341.
- Ibbetson, A. & Phillips, N. 1967 Some laboratory experiments on Rossby waves in a rotating annulus. *Tellus* **19**, 81–87.
- Lamb, H. 1932 *Hydrodynamics*, 6th ed. Cambridge University Press.
- Longuet-Higgins, M. S. 1969 On the trapping of long-period waves round islands. *J. Fluid Mech.* **37**, 773–784.
- Longuet-Higgins, M. S. 1970 Steady currents induced by oscillations round islands. *J. Fluid Mech.* **42**, 701–720.
- Longuet-Higgins, M. S. 1971 On the spectrum of sea level at Oahu. *J. geophys. Res.* **76**, 3517–3522.
- Miyata, M. & Groves, W. G. 1968 Note on sea level observations at two nearby stations. *J. geophys. Res.* **73**, 3965–3967.
- Phillips, N. 1965 Elementary Rossby waves. *Tellus* **17**, 295–301.

- Rattray, M. & Charnell, R. L. 1966 Quasi-geostrophic free oscillations in enclosed basins. *J. mar. Res.* **24**, 82-102.
- Summerfield, W. 1972 Circular islands as resonators of long-wave energy. *Phil. Trans. R. Soc. Mond. A* **272**, 361-402.
- Wilcox, S. D., Eide, S. A. & Caldwell, D. R. 1974 Adapting small dc motors for precise speed control. *Rev. sci. Instrum.* **45**, 510-512.